



## Research Paper

## Experimental investigation of the performance attributes of a double pipe heat exchanger equipped with baffles of conventional or flower layouts



Mohamed R. Salem\*, Mohamed M. Ellaban, R.K. Ali, Ashraf E. Elmohlawy

*Mechanical Engineering Department, Faculty of Engineering at Shoubra, Benha University, 108 Shoubra St., 11629, Cairo, Egypt*

## ARTICLE INFO

**Keywords:**

Double pipe heat exchanger  
 Segmental baffles  
 Flower baffles  
 Heat transfer augmentation  
 Performance

## ABSTRACT

In industrial heat management, the design of baffles within heat exchangers is crucial. They guide fluid flow and enhance turbulence, optimizing heat transfer. Yet, their configuration must be carefully considered to balance thermal efficiency with energy expenditure and pressure management. This research conducts practical tests on the hydrothermal attributes of a counter-flow double-pipe heat exchanger. It evaluates two baffle layouts: segmental and flower, considering baffle cut-off ratio ( $16.7\% \leq \delta \leq 50\%$ ), pitch ratio ( $8.3\% \leq \lambda \leq 22.2\%$ ), flower-design relative angle ( $30^\circ \leq \gamma \leq 90^\circ$ ), and operating conditions of annulus-side ( $2660 \leq Re_{an} \leq 13110$ ,  $5.21 \leq Pr_{an} \leq 7.48$ ). The findings assure that installing the baffles results in notable increases in both  $\bar{Nu}_{an}$  and  $f_{an}$ . Besides, lowering baffle cut-off and pitch ratios, and increasing the relative angle of flower baffles lead to additional increases. Moreover, raising the annulus-fluid temperature reduces  $\bar{Nu}_{an}$  with a negligible effect on  $f_{an}$ . Increasing  $Re_{an}$  leads to a reduced  $f_{an}$  and greater  $\bar{Nu}_{an}$ . Compared with no baffles, the maximum recorded increases in the  $\bar{Nu}_{an}$  and  $f_{an}$  are 147.4 % and 60.2 %, respectively, realized by incorporating flower layout. On average, the flower baffles boost the  $\bar{Nu}_{an}$  by 20.8 % more than those using conventional baffles, with an average increase of 4.3 % in the  $f_{an}$ . To judge the benefit of utilizing baffles, the Hydrothermal Performance Index (*HTPI*) is calculated, and its highest value is recorded as 2.23, attained by running the annular pipe at the lowest flow rate and temperature, with inserting flower baffles ( $\delta = 16.7\%$ ,  $\lambda = 8.3\%$ ,  $\gamma = 90^\circ$ ). Finally, correlations for  $\bar{Nu}_{an}$ , *HTPI*, and  $f_{an}$  prediction are suggested.

## 1. Introduction

The phenomenon of heat transfer stands as a cornerstone in a multitude of applications spanning air conditioning systems, power generation facilities, industrial operations, and combustion mechanisms. These applications hinge on the pivotal process of transferring thermal energy from a warmer fluid to a cooler one, harnessing this energy for operations integral to our daily existence. At the heart of this process lies the heat exchanger, a device celebrated for its myriad configurations, each designed to facilitate this crucial energy exchange. The efficiency of this process is not without cost implications; it accounts for a substantial portion of both the capital and operational expenditures. These costs are attributed to the need for adequate surface area to enable effective heat transfer and the requisite pumping power to circulate the fluids at an optimal rate. Thus, enhancing the rate of heat transfer while concurrently reducing the volume of the heat exchanger and mitigating the pressure drop associated with fluid flow is paramount. Achieving

these objectives is essential for optimizing the performance of heat exchangers and fulfilling the stringent heat transfer requisites set forth by various applications [1,2].

Improving the performance of heat exchangers can be approached through various strategies, broadly categorized into active and passive techniques. Passive methods, such as the implementation of fins, additives, coiled tubes, baffles, and more, are favored for their independence from external power sources [3]. Among these, baffles of assorted designs are prevalently utilized due to their ease of installation and their significant contribution to elevating heat transfer rates. Nonetheless, this improvement is often accompanied by an uptick in the working fluid's friction coefficient, which is intrinsically linked to a myriad of geometric design parameters of the baffles [4]. Consequently, the geometric shape of baffles has become a focal point of research interest, prompting numerous studies to investigate its effects. Lei et al. [5] numerically and experimentally investigated a heat exchanger with single-helical baffles, revealing that it has 75 % heat transfer capacity but only 50 % pressure drop, contrasting with the heat exchanger with

\* Corresponding author at: Mechanical Engineering Department, Faculty of Engineering at Shoubra, Benha University, 108 Shoubra St., 11629, Cairo, Egypt.  
 E-mail address: [mohamed.abdelhamid@feng.bu.edu.eg](mailto:mohamed.abdelhamid@feng.bu.edu.eg) (M.R. Salem).

<b>Nomenclature</b>		<i>Re</i>	Reynolds number
<i>A</i>	Area,m <sup>2</sup>	<i>St</i>	Stanton number
<i>C p</i>	Specific heat,J/kg. °C		
<i>d</i>	Diameter, m		
<i>f</i>	Fanning friction factor		
<i>h̄</i>	Convection heat transfer coefficient,W/m <sup>2</sup> . °C		
<i>k</i>	Thermal conductivity,W/m. °C		
<i>L</i>	Length, m		
<i>m̄</i>	Mass flow rate,kg/s		
<i>N</i>	Number of baffles		
<i>P</i>	Pressure, Pa		
<i>p</i>	Baffle pitch, mm		
<i>Q</i>	Heat transfer rate, W		
<i>T</i>	Temperature, °Cor K		
<i>t</i>	Time, s		
<i>U</i>	Overall heat transfer coefficient,W/m <sup>2</sup> . °C		
<i>V</i>	Volume,m <sup>3</sup>		
<i>̄V</i>	Volume flow rate,m <sup>3</sup> /s		
<i>Dimensionless groups</i>			
<i>Nū</i>	Average Nusselt number		
<i>Pr</i>	Prandtl number		
<i>Greek letters</i>			
$\lambda$	Baffle pitch ratio		
$\Delta$	Differential		
$\omega$	Uncertainty		
$\gamma$	Baffle relative angle, °		
$\delta$	Baffle cut-off ratio		
$\pi$	Pi ≡ A mathematical constant ≈ 3.1416		
$\rho$	Density,kg/m <sup>3</sup>		
<i>Superscripts and subscripts</i>			
<i>an</i>	Annulus		
<i>ave</i>	Average		
<i>h</i>	Hydraulic		
<i>i</i>	Inlet/Inner/Internal		
<i>LM</i>	Logarithmic mean		
<i>o</i>	Out/Outer		
<i>t</i>	Tube		
<i>Acronyms and abbreviations</i>			
<i>HTPI</i>	Hydrothermal Performance Index		

single-segmental baffles. In their study, Zhang et al. [6] examined how shell-tube heat exchangers functioned with different types of baffles. They discovered that using helical baffles resulted in a reduced pressure drop and less effective heat transfer compared to segmental baffles. Targui and Kahalerras [7] conducted a numerical investigation into the application of single-segmental porous baffles along with pulsating flow within double-pipe heat exchangers. Results showed that the flow structure significantly affected the effectiveness of the heat exchanger. The study suggested that combining porous baffles and pulsating flow was promising for improving thermal system performance. Hussein [8] explored the effects of turbulent flow and heat transfer in a concentric tube heat exchanger that incorporated semicircular disc baffles. The experimental data suggested that the most efficient baffle spacing was 15 cm, which also led to higher values of the Nusselt number and friction factor, influenced by the baffle spacing and the mass flow rate of the fluid. Zhou et al. [9] analyzed heat transfer and fluid flow in a shell-and-tube heat exchanger with trefoil-hole baffles, finding good agreement with experiments. The fluid flowed periodically, with gradients in temperature and pressure recurring. The fluid fully developed after the first baffle, and the velocity decreased gradually, resulting in a decrease in the average convective heat transfer coefficient. El Maakoul et al. [10] numerically investigated the effect of installing trefoil-hole, helical, and segmental baffles on the hydrothermal performance attributes of shell-tube heat exchangers. It was found that the helical type provided the highest performance, while the trefoil-hole type was associated with the highest heat transfer and pumping power.

Gu et al. [11] predicted the thermal performance of a shell-tube heat exchanger by incorporating shutter and segmental baffles in a triangular configuration. It was documented that the shutter layout results in higher performance than the segmental configuration. Besides, the baffle pitch and strip inclination angle had a great effect on the performance attributes. Aniket et al. [12] considered segmental, helical, and flower baffles during their simulations. The study found that single-segmental baffles have the highest pressure drop and heat transfer rate, while helical baffles have almost zero stagnation zones, and flower-type baffles have reduced stagnation zones. Amirtharaj et al. [13] performed numerical simulations to examine how a heat exchanger would function if it had inclined baffles rather than segmented ones. The findings showed that there was a modest 2.5 % decrease in pressure drop and a

12 % increase in heat transfer rate. Sheikholeslami and Ganji [14] examined the operation of a double pipe heat exchanger by incorporating perforated turbulators within the annular space. The study focused on evaluating the system's efficiency, considering parameters such as pitch ratio, open area ratio, and Reynolds number. The findings revealed that enhancing the open area ratio led to improved thermal performance. Kumar et al. [15] explored turbulence-induced heat transfer in heat exchanger tubes using a circular perforated ring insert, revealing a fourfold heat transfer enhancement and a 1.47 times thermal performance improvement. Mellat et al. [16] numerically revealed that baffle orientation and spacing between baffles significantly affect the shell side thermal performance of a heat exchanger, resulting in a 3.55-factor improvement. Salem et al. [17] practically looked into the features of double-pipe heat exchangers with and without perforated baffles in terms of hydrothermal performance. The findings showed that the baffles' cut, pitch, and perforation ratios significantly affected the rate of heat transfer and flow pumping power. Wena et al. [18] used particle image velocimetry to test the shell-side flow patterns in shell and tube heat exchangers with helical baffles in an experimental setting. According to the experiments, the upgraded heat exchanger's performance increased by 8 %. Zhang et al. [19] numerically developed a shell-and-tube heat exchanger with screw cinquefoil orifice baffles to enhance heat transfer coefficient and fluid cleansing ability. The design improved fluid flushing and introduced a 9.2 % higher heat transfer coefficient under the same flow rate. To compare the effect of inserting baffles with various designs on the performance of shell and tube heat exchangers, Bichkar et al. [20] ran numerical simulations. The results demonstrated that helical baffles had the lowest pumping power, while single-segmental baffles had the most pressure loss. Besides, double segmental baffles eliminated dead zones and prevented vibrational damage. Salem et al. [2] tested concentric tube heat exchangers with a helical tape insert, finding it increased friction factor and annulus average Nusselt number compared to the simple annulus case.

Colaço et al. [21] applied a differential evolution algorithm to optimize heat exchanger efficiency in five scenarios and 11 cases, demonstrating its correctness through numerical analysis. Amini et al. [22] performed a numerical analysis that revealed that vertical segmented tube fins and helical fin design significantly enhanced the shell-and-tube heat exchanger's thermal performance, boosting its

efficiency by 6 % and 9.5 %, respectively. Wang et al. [23] performed a numerical simulation of a heat exchanger's operation for three different baffle layouts: segmental, continuous helical, and staggered. The authors demonstrated that the best results were obtained with staggered baffles. Petinrin and Dare [24] looked into how well shell-and-tube heat exchangers with concave-cut and single-segmental baffle layouts performed. The findings demonstrated that concave-cut baffles performed less well than single-segmental baffles, with larger pressure drops and worse performance factors. Ajeel et al. [25–32] conducted a series of experimental and numerical studies considering the flow of numerous types of nanofluids through corrugated channels. During the analyses, three different designs of corrugations: semicircle, trapezoidal, and straight were evaluated. The authors identified the optimal geometrical parameters for each case and found that the combination of silica nanofluid and trapezoidal layout provided the highest augmentation in heat exchange. Thejaraju et al. [33] examined the impact of louvered winglet tape in enhancing heat exchange in double pipe systems. They revealed that optimal heat transfer occurs at specific angles and flow rates, offering promising efficiency improvements for heat transfer applications. Bensaci et al. [34] performed a computational and experimental investigation on the position of baffles in a solar air heater. The revised baffle placements demonstrated that successful thermohydraulic performance was not solely determined by the shape of the baffles or changes in their geometric properties. The proper positioning of baffles significantly increased the thermohydraulic performance of solar air heaters. Mohammadi et al. [35] investigated the pressure drop and heat transmission in a porous baffled shell and tube heat exchanger. They showed that low-cut baffles increased pressure loss but enhanced heat transfer. The ideal parameters were trained into an artificial neural network to maximize heat transmission and minimize pressure drop. Mahendran [36] utilized both experimental validation and numerical analysis to study the operation of a shell-and-tube heat exchanger with flower plate baffles. In comparison to a conventional heat exchanger, the suggested heat exchanger provided more effective cooling. Kumar et al. [37] introduced a study on the effects of hemispherical turbulators in a double-pipe heat exchanger. It highlighted that while turbulators increased heat transfer, they also raised the friction factor. A maximum performance indicator of 1.41 was recorded. Nakhchi et al. [38] explored double-pipe heat exchangers with perforated inclined elliptic turbulators, showing a 217.4 % increase in Nusselt number and 39.4 % better heat transfer, achieving a thermal efficiency of 1.85 without significant friction loss. In their shell-and-tube heat exchanger performance model, Youcef and Saim [39] determined minor dead zones at 40° baffle inclination, but a greater baffle angle resulted in lower performance factors.

Gaikwad and Parmar [40] simulated a shell-and-tube heat exchanger with segmental baffles, finding a 13.1 % increase in heat transfer coefficient. Chen et al. [41] developed a shell-and-tube heat exchanger with triple-layer flower baffles. Results showed that triple-layer and double-layer baffles increased shell-side heat transfer coefficients by 31.7 % and 14.3 %, respectively, compared to traditional segmental baffles. Ajeel et al. [42] numerically analyzed a curved-corrugated channel with E-shaped baffles and ZnO-water nanofluid, finding baffle-equipped channels perform better than without, especially at 10° pitch angle, with an optimal thermal-hydraulic performance factor of 2.57. In another research, Ajeel et al. [43] numerically examined the behavior of fluid movement and the effectiveness of heat transfer in a curved-corrugated channel with ZnO-water nanofluid and L-shaped baffles. The results demonstrated that the formation of vortex flow and the amplification of turbulence considerably improved the heat transfer process. Furthermore, it was determined that arranging baffles in an inline pattern optimized thermal-hydraulic efficiency. Ajeel et al. [44] extended their works by using a binary hybrid (CuO/MgO-water) nanofluid to improve flow and heat transfer in E-shaped baffled curved-corrugated channel, resulting in a 72 % improvement in Nusselt number and 32 % increase in friction factor. Sahel [45] conducted a

computational analysis on the effectiveness of flower baffles in a tubular heat exchanger. Findings revealed that incorporating flower baffles enhanced the mixing of air and disrupted areas of stagnation behind the baffles, thereby significantly elevating the efficiency of heat exchange. Colaço et al. [46] used a reinforcement learner non-dominated sorting genetic algorithm to design a double pipe heat exchanger with perforated baffles. The study found that internal perforated baffles significantly improved heat transfer, with a Nusselt number and friction factor increasing by 7.9 – 8.3 times compared to a plain double pipe heat exchanger. Kaleru et al. [47] designed a shell and tube heat exchanger using segmental and helical baffles, comparing the Nusselt number and friction factor, finding segmental baffles superior in terms of the Colburn factor. Through the imposition of trefoil holes on segmental baffles, Saad et al. [48] introduced a segmented trefoil baffle, which exhibited superior thermohydraulic performance, a large reduction in dead zones, and a reduction in pressure loss, according to numerical simulations. The effect of V-shaped delta-wing baffles was tested experimentally by Samruaisin et al. [49]. Based on the findings, the Nusselt number might be increased by up to 97 – 105.6 % due to the high heat transfer rates provided by more wings. Multi-vortex flows produced by the baffles additionally mixed the fluid. Kumar et al. [50] presented a numerical study on the use of truncated conical turbulators in double pipe heat exchangers, demonstrating that these turbulators could pointedly boost thermohydraulic efficiency up to 1.13. Ji et al. [51] investigated the impact of baffle structure on elastic tube bundle heat exchanger performance. Results showed that increasing baffle height reduced vibration and enhanced heat transfer performance. The highest vibration intensity occurred at 10° baffle curvature, resulting in a 10.8 % improvement in amplitude. The impact of adding segmental baffles with two distinct cutting patterns (internal and edge) and nanoparticles on the heat exchanger's shell side was experimentally investigated by Almulla et al. [4,52]. The outcomes showed that the edge cut outperformed the interior cut in terms of performance and that the best performance was attained by combining the use of baffles and nanofluid. Banihashemi et al. [53] explored the use of moving turbulators in heat exchangers, comparing them to stationary ones. They concluded that rotating turbulators, especially those with lower angle ratios, significantly enhanced thermal efficiency and outperformed their stationary counterparts.

This scholarly review uncovers a plethora of research centered on the dynamic effects of integrating baffles with diverse geometries into heat exchangers. A significant portion of these studies have delved into the impact of segmental baffle configurations on the attributes of fluid dynamics. It is well-documented that the baffle's structural design, its angular placement, the precise ratio of its cut, and the interval between baffles are critical determinants that substantially modify the heat transfer dynamics and the associated pressure drop. Furthermore, recent investigations have highlighted the enhanced efficiency of flower baffles in elevating heat exchanger performance. Yet, these explorations have not fully examined the influence of the flower baffle's geometric details on hydrothermal performance indicators.

Considering these findings, this research proposes to undertake a detailed experimental examination of the hydrothermal characteristics inherent to a counter-flow double-pipe heat exchanger, outfitted with either single-segmental or flower baffles within its annular domain. The study scrutinizes the influence of variations in baffle cut and pitch ratios, as well as the flower design's angular orientation, under a wide spectrum of operational conditions affecting the annulus. The ambition of this investigation is to establish empirical correlations that facilitate the prediction of the average Nusselt number ( $\overline{Nu}_{an}$ ) and Fanning friction factor ( $f_{an}$ ) for the annulus when utilizing both types of baffles. Additionally, it aims to introduce a hydrothermal performance index ( $HTPI$ ) that quantifies the effectiveness of the heat exchanger employing this innovative methodology, in contrast to conventional heat exchanger configurations.

## 2. Experimental apparatus

The apparatus used in this study comprises heating and cooling water paths, with the heating water loop including a heating unit, a centrifugal pump, ball valves, the internal copper tube, a rotameter, and connections. A cooling water path involves a centrifugal pump, ball valves, the outer pipe (annulus side), a rotameter, and connections. Figs. 1 & 2 demonstrate both paths and the overall system. Two insulated 50-liter tanks are utilized for the cooling and heating systems. To heat the water to the required temperature (70 °C), two 5 kW electric heaters are employed in the heating tank. Two vapor compression refrigeration systems with a total capacity of 10.5 kW are integrated with the cooling tank to cool the water to the desired temperature. Digital thermostats are used to regulate the operation of the heating and cooling units, ensuring constant temperatures for liquids flowing to the heat exchanger. Two ports are fabricated in the top cover of each tank to receive the water coming from the heat exchanger and the bypass line. Two ports are fabricated at the bottom of each tank to deliver the water to the heat exchanger and the drain line. Two 1.5-hp centrifugal pumps are engaged to move the working fluids in their loops. The annulus main line and a differential pressure transducer are connected using PVC and flexible nylon connections.

The volume flow rates of hot and cold water on both sides of the heat exchanger are measured with an accuracy of 5 % using two calibrated rotameters (1.7–18 L/min). Approximately 5 cm away from the ports of the heat exchanger, four K-type thermocouples are positioned within the flow to measure the temperatures at the entry and exit points of both the annular space and the internal tube's fluids. A digital thermometer featuring 0.1 °C resolution is used to display their readings. Besides, a calibrated digital transducer with a 1 % accuracy range (0–103.4 kPa) is used to quantify the pressure differential at the annulus ends.

Thirteen concentric tube heat exchangers with counter-flow configurations are designed and built: one is a simple heat exchanger without baffles, and the other twelve heat exchangers are made with various

baffle layouts; conventional segmental or flower, as demonstrated in Table 1. The baffles are made of a 2 mm-thick acrylic sheet, and they are cut using a laser machine. All baffles are circular and have the same diameter as the heat exchanger annular pipe. The heat exchanger's annular pipe is composed of a seamless black steel tube with an internal diameter of 56 mm and a wall thickness of 4 mm. PVC caps are utilized to seal their ends. Every exchanger has an interior copper tube that is 1800 mm effective length, with external and internal diameters of 22 mm and 20 mm, respectively. Thick layers of glass wool, asbestos rope, and ceramic fibre provide thermal isolation to the exterior of every annular pipe. Fig. 3 shows cross-sectional and 3D views of the baffle inside the annulus of the heat exchanger, and Table 1 reveals the typical dimensions of the various configurations.

The cut-off ratio ( $\delta$ ) is defined through Eq. (1) using the total unoccupied area ( $A_{cut}$ ) in each baffle, which is assessed using SolidWorks program. As well, the baffle pitch ratio ( $\lambda$ ) is recognized via Eq. (2) as the ratio between the pitch between the baffles ( $p_{baffle}$ ) and the tube length ( $L_t$ ), while the relative angle ( $\gamma$ ) expresses the angle between the centreline of the cuts for two consecutive baffles, as indicated in Fig. 4.

$$\delta = \frac{4A_{cut}}{\pi d_{an}^2} \quad (1)$$

$$\lambda = \frac{p_{baffle}}{L_t} \quad (2)$$

## 3. Experimental procedures

First, the inlet and exit of the annulus, as well as the tube sides, are fitted with thermocouples. The tests then begin with the assembly of the double-pipe heat exchanger, pumps, pipelines, heating and cooling units, flow meters, thermocouples, and a differential pressure transducer. The heating and cooling tanks are filled with water from the home water supply. The pumps, cooler, and heater are then turned on. There are 273 experiments performed on the thirteen heat exchangers.

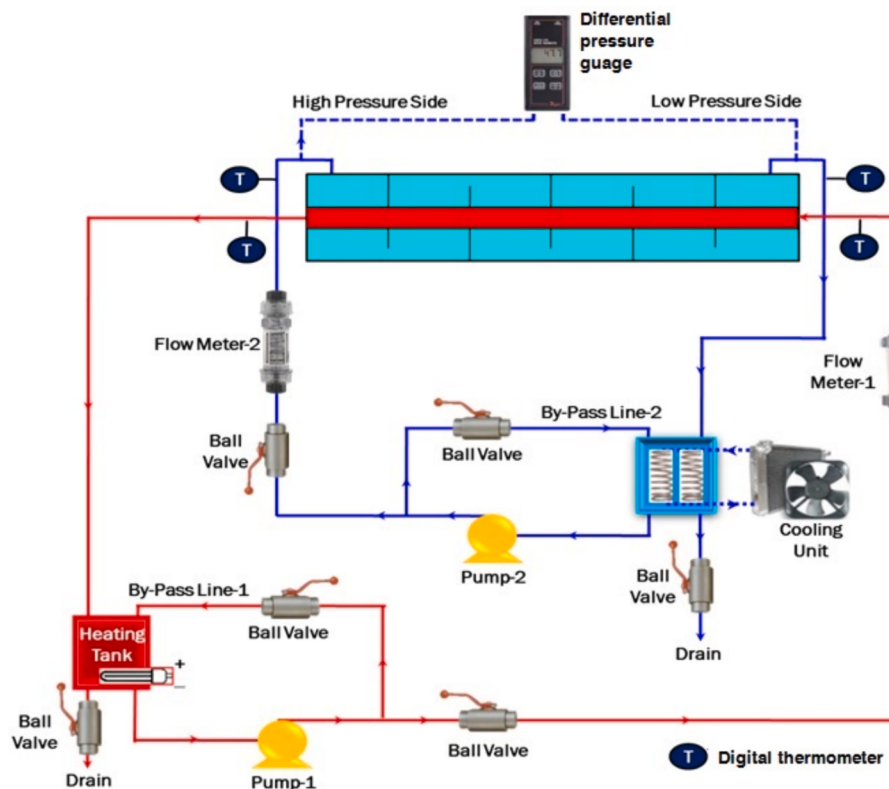


Fig. 1. Schematic diagram of the experimental setup.



Fig. 2. A photo of the present setup.

**Table 1**  
Key parameters of the examined heat exchangers.

#	Baffle Layout	Cut-off Ratio ( $\delta$ )	$N_{\text{baffle}}$	Pitch (mm)	Pitch Ratio ( $\lambda$ )	Relative Angle ( $\gamma$ )
1	No baffles	—				
2	Segmental	50.0 %	9	200	11.1 %	180°
3		33.3 %				
4		16.7 %	5	400	22.2 %	
5			9	200	11.1 %	
6			12	150	8.3 %	
7	Flower	50.0 %	9	200	11.1 %	90°
8		33.3 %				
9		16.7 %	9	200	11.1 %	30°
10						60°
11			5	400	22.2 %	90°
12			9	200	11.1 %	
13			12	150	8.3 %	

When the fluid intake and exit temperatures are constant and their variations are around 0.1 °C, the test procedure is deemed to be in a steady-state condition, and these measured values are now being recorded. Table 2 provides the range of the operational conditions.

#### 4. Calculation methodology

Six variables make up the primary measurements used in heat transfer estimations: the flow rates and the temperatures of the heat exchanger's inlet and exit. Eqs. (3) and (4) are used to evaluate the heat transfer rates ( $Q_t$  and  $Q_{an}$ ) on the tube and annulus sides. If the measurements are exact enough and there is no heat gain or loss, there should be an energy balance between the two rates ( $Q_t = Q_{an}$ ). However, there are some differences between them in the tests. As a result,  $Q_{ave}$ , the mean value, is determined through Eq. (5) and employed during calculations. It should be noted that by applying Eq. (6), the heating and cooling loads from the hot and cold sides did not differ by more than ± 3.9 % for all runs. This  $Q_{ave}$  is then used to assess the overall thermal conductance ( $U_i A_{t,i}$ ) via Eq. (7), in which the logarithmic temperature difference ( $\Delta T_{LM}$ ) and the area of the internal surface of the tube ( $A_{t,i}$ ) are estimated through Eqs. (8) and (9), respectively.

$$Q_t = \dot{m}_t C p_t (T_{t,i} - T_{t,o}) \quad (3)$$

$$Q_{an} = \dot{m}_{an} C p_{an} (T_{an,o} - T_{an,i}) \quad (4)$$

$$Q_{ave} = \frac{|Q_t| + |Q_{an}|}{2} \quad (5)$$

$$\Delta Q_{ave}(\%) = \frac{|Q_t| - |Q_{an}|}{Q_{ave}} \times 100 \quad (6)$$

$$U_i A_{t,i} = \frac{Q_{ave}}{\Delta T_{LM}} \quad (7)$$

$$\Delta T_{LM} = \frac{(\Delta T_1 - \Delta T_2)}{\ln \left[ \frac{\Delta T_1}{\Delta T_2} \right]} = \frac{(T_{t,i} - T_{an,o}) - (T_{t,o} - T_{an,i})}{\ln \left[ \frac{T_{t,i} - T_{an,o}}{T_{t,o} - T_{an,i}} \right]} \quad (8)$$

$$A_{t,i} = \pi d_{t,i} L \quad (9)$$

The tube length (1800 mm) is 90 times its hydraulic diameter ( $d_{t,i} = 20$  mm), therefore, water flow in the internal tube is fully developed. Applying the Dittus-Boelter [54] correlation, Eq. (10), yields the average Nusselt number of the tube-side ( $\bar{Nu}_t$ ), which is substituted into Eq. (11) to assess the heat transfer coefficient on the tube side ( $\bar{h}_t$ ). The Dittus-Boelter correlation is valid for  $L_t/d_t \geq 60$ ,  $0.7 \leq Pr_t \leq 100$ , and  $Re_t \geq 10000$ . At this time, Eq. (12) can be used to predict the heat transfer coefficient on the annulus side ( $\bar{h}_{an}$ ). Besides, the average Nusselt number and Fanning friction factor of the annulus side are estimated through Eqs. (13) and (14), respectively. It should be noted that Eq. (15) is utilized to assess the hydraulic diameter of the annulus side ( $d_{an,h}$ ), while Eqs. (16) and (17) are applied to estimate the Reynolds numbers on the tube and annulus sides, respectively.

$$\bar{Nu}_t = 0.023 Re_t^{0.8} Pr_t^{0.4} \quad (10)$$

$$\bar{h}_t = \frac{\bar{Nu}_t k_t}{d_{t,i}} \quad (11)$$

$$\bar{h}_{an} = \left[ \frac{A_{t,o}}{U_i A_{t,i}} - \frac{A_{t,o}}{\bar{h}_t A_{t,i}} \right]^{-1} \quad (12)$$

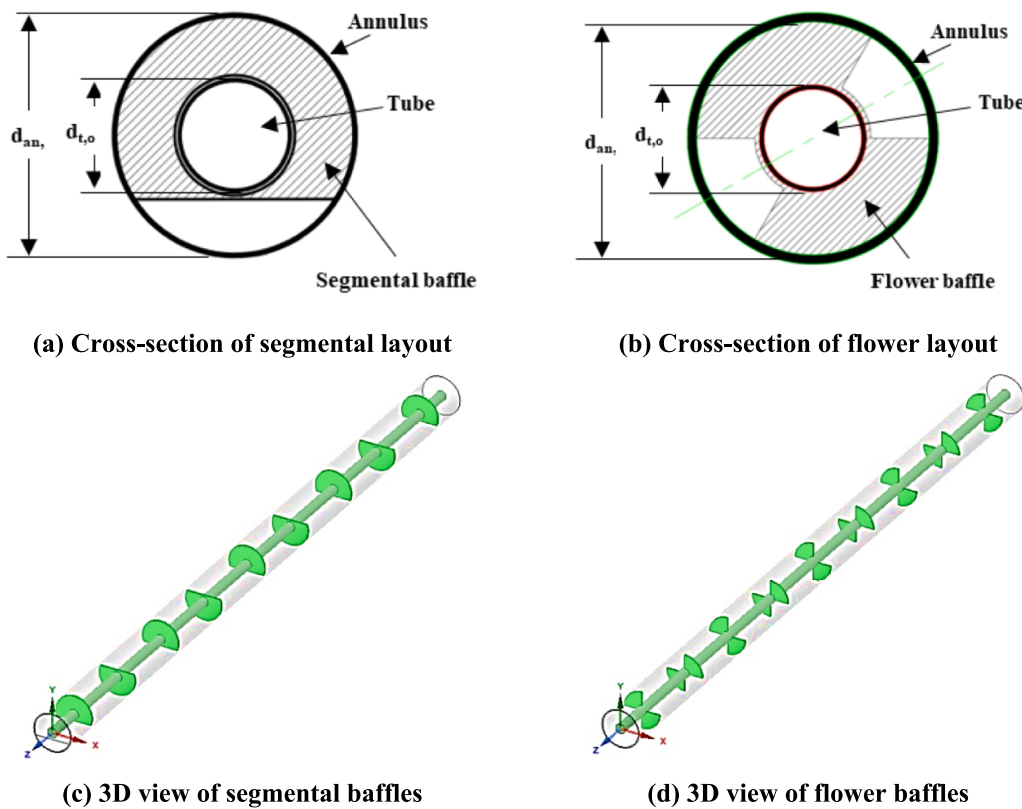


Fig. 3. Schematic representation of the baffles in the heat exchanger.

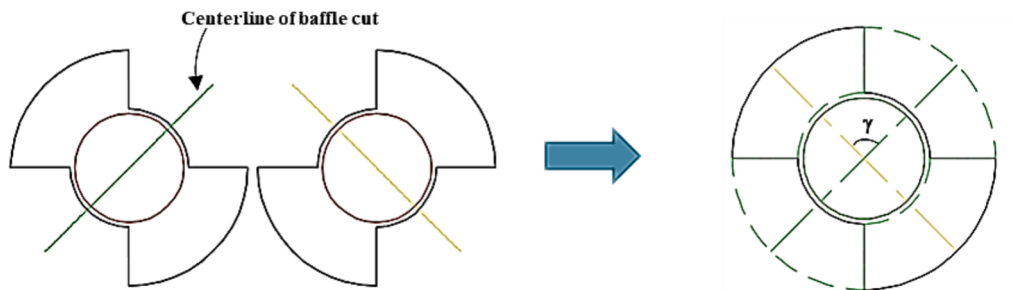


Fig. 4. Representation of the relative angle between two consecutive flower baffles.

**Table 2**  
Range of the operating conditions in the heat exchanger.

Parameters	Range or value
Annulus-side flow rate, L/min	4.1 – 16.3 ( $2660 \leq Re_{an} \leq 13110$ )
Annulus-side inlet temperature, °C	15, 20, 25 ( $5.21 \leq Pr_{an} \leq 7.48$ )
Tube-side flow rate, L/min	8.1 ( $Re_t \cong 19300$ )
Tube-side inlet temperature, °C	70 ( $Pr_t \cong 2.76$ )

$$\overline{Nu}_{an} = \frac{\bar{h}_{an} d_{an,h}}{k_{an}} \quad (13)$$

$$f_{an} = \frac{\Delta P_{an} \pi^2 \rho_{an} d_{an,h}^5}{32 L_{an} m_{an}^2} \quad (14)$$

$$d_{an,h} = d_{an,i} - d_{t,o} \quad (15)$$

$$Re_t = \frac{4\dot{m}_t}{\pi d_{t,i} \mu_t} \quad (16)$$

$$Re_{an} = \frac{4\dot{m}_{an}}{\pi d_{an,h} \mu_{an}} \quad (17)$$

## 5. Uncertainty analysis

This study uses laboratory data and physical features to evaluate the experimental results. Calculating an accurate uncertainty factor requires taking measurement errors into account. Accuracy is necessary for sensor precision and can be attained by following manufacturer standards or calibration guidelines. Regarding the internal tube diameter, the manufacturer's margin of error is  $\pm 0.05$  mm; for the other specified dimensions, the uncertainty is  $\pm 0.5$  mm. Moreover, a tolerance of  $\pm 0.1$  % is applied to the thermophysical uncertainties of the cooling/heating water. Table 3 summarizes the methods used by Kline and McClintock [55] to determine the uncertainty of the major parameters. Appendix A provides more details.

**Table 3**  
Max. uncertainties in the key parameters.

Parameter	Uncertainty (%)
Annulus-side Reynolds number	±1.69
Tube-side Reynolds number	±1.91
Annulus-side average Nusselt number	±3.15
Annulus-side average heat transfer coefficient	±3.02
Tube-side average Nusselt number	±1.35
Tube-side average heat transfer coefficient	±1.71
Overall heat transfer coefficient	±4.46
Annulus-side Fanning friction factor	±5.67
Hydrothermal performance index	±5.90

## 6. Apparatus validation and data verification

To validate the heat transfer and friction coefficients, the flow and temperature data on the annulus side are monitored, and the  $\bar{Nu}_{an}$  and  $f_{an}$  are compared to established correlations in accordance with the working circumstances specified in [Table 4](#). The  $\bar{Nu}_{an}$  is compared to Gnielinski [56], Eq. (18), while the  $f_{an}$  is compared with Filonenko's correlation [57], Eq. (19). The comparisons reveal consistent results for the determination of  $\bar{Nu}_{an}$  and  $f_{an}$ , with maximum variances of 7.2 % and 5.5 %, respectively, as presented in [Fig. 5](#). This indicates that the experimental apparatus and measuring techniques, besides the calculation methodology, are appropriate.

$$\bar{Nu}_{an} = \frac{\frac{f_{an}}{2} (Re_{an} - 1000) Pr_{an}}{1 + 12.7 \sqrt{\frac{f_{an}}{2}} (Pr_{an}^{2/3} - 1)} \left[ 1 + \left( \frac{d_{an,h}}{L_{an}} \right)^{2/3} \right] \quad (18)$$

$$f_{an} = 0.25 (1.82 \log Re_{an} - 1.64)^{-2} \quad (19)$$

## 7. Results and discussions

### 7.1. Effect of cut-off ratio of the baffles

In this analysis, the effect of the baffle cut-off ratio is investigated. The experiments are carried out using both baffle layouts: segmental and flower, for  $\delta = 16.7\%$ ,  $33.3\%$ , and  $50\%$ . Baffles with a fixed pitch (200 mm) are integrated into the annular side of the heat exchanger with a corresponding pitch ratio of  $\lambda = 11.1\%$ . The operating conditions are applied as indicated in [Table 2](#). [Figs. 6 and 7](#) show a sample of the findings for  $\bar{Nu}_{an}$  and  $f_{an}$  at  $T_{an,i} = 20^\circ\text{C}$ .

It is evident that once baffles are installed on the annular side of the heat exchanger, both the Nusselt number and friction coefficient increase significantly, whether using conventional baffles or the proposed flower design. Besides, these increases are raised by decreasing the cut-off ratio of the baffle. Under all operating conditions during these experiments, compared to no baffles, the average increases in  $\bar{Nu}_{an}$  are 87.1 %, 61.2 %, and 39.1 % by installing segmental baffles with cutoff ratios of 16.7 %, 33.3 %, and 50 %, respectively. Additionally, by integrating the flower layout with a relative angle of 90°, the corresponding average increases in  $\bar{Nu}_{an}$  are 128.3 %, 83.5 %, and 60.2 %, respectively. Furthermore, the associated average increases in the  $f_{an}$  are 52.0 %, 35.1 %, and 22.4 %, respectively, with engaging segmental layout, and 55.5 %, 37.5 %, and 27.3 %, respectively, with engaging flower design.

**Table 4**  
Specifications of the validation process.

Parameters	Range or value
Annulus-side flow rate, L/min	4.1 – 16.3 ( $2985 \leq Re_{an} \leq 12835$ )
Annulus-side inlet temperature, °C	15, 20, 25 ( $5.59 \leq Pr_{an} \leq 7.48$ )
Tube-side flow rate, L/min	8.1 ( $Re_t \cong 19715$ )
Tube-side inlet temperature, °C	70 ( $Pr_t \cong 2.69$ )

These results are indicative of an intensified throttling effect that the fluid endures within the annular space. This effect is heightened as the fluid passes through areas where baffles are intentionally placed to create resistance. The presence of baffles induces a significant increase in fluid velocity and a corresponding decrease in pressure, which in turn generates turbulence within the fluid flow. The concept of throttling is inversely related to the cut-off ratio, which is a measure of the flow restriction within a channel. A lower cut-off ratio signifies a greater restriction, which naturally leads to increased turbulence. This turbulence is characterized by chaotic fluid motion, which includes the formation of eddies that promote thorough mixing of the fluid layers. As the fluid's turbulent motion disrupts the orderly flow, it also begins to dismantle the established thermal boundary layer. This layer typically acts as an insulator, reducing the rate of heat transfer. However, when this layer is disturbed, the insulation effect is diminished, allowing for a more direct and efficient transfer of heat. The combined effects of increased turbulence, the breakdown of the thermal boundary layer, and the enhanced mixing of fluid layers significantly improve the overall heat transfer efficiency. However, these benefits come with a trade-off, a noticeable increase in the pressure drop across the annular space. This pressure drop is a critical factor in the design and operation of heat transfer systems, as it can impact the overall energy efficiency and performance.

### 7.2. Effect of pitch ratio of the baffles

In this investigation, the influence of the baffle pitch ratio on the heat exchanger performance parameters is studied. The experiments are also conducted utilizing both baffle configurations: the segmental and flower layouts, for three different longitudinal distances of  $\lambda = 8.3\%$ ,  $11.1\%$ , and  $22.2\%$ . Notably, the baffles integrated into the annular side of the heat exchanger have a consistent cut-off ratio of 16.7 %, ensuring a standard comparison across the experiments. The prescribed operating conditions detailed in [Table 2](#) are consistently adhered to throughout the experimental procedures. [Figs. 8 and 9](#) display a sample of the findings for  $\bar{Nu}_{an}$  and  $f_{an}$  at  $T_{an,i} = 15^\circ\text{C}$ .

It is important to note that the impact of installing baffles on the annular side of the heat exchanger is quite significant, leading to notable increases in both  $\bar{Nu}_{an}$  and  $f_{an}$  values. This holds for both conventional baffles and the innovative flower design. Notably, the magnitude of these increases is further raised by reducing the pitch ratio of the baffle. Comparing this with scenarios where no baffles are utilized, the improvements in  $\bar{Nu}_{an}$  are substantial, standing at 104.8 %, 87.1 %, and 73.6 % for  $\lambda$  values of 8.3 %, 11.1 %, and 22.2 % in the conventional segmental configuration, while the flower layout sees improvements of 147.4 %, 128.3 %, and 117 %. Similarly, the corresponding increases in  $f_{an}$  are 53.7 %, 52 %, and 43.5 % for segmental baffles at  $\lambda$  values of 8.3 %, 11.1 %, and 22.2 %, respectively, and 60.2 %, 55.5 %, and 49.2 % when employing flower baffles. These findings emphasize the importance of baffle design and configuration in enhancing the performance of the heat exchanger system.

Decreasing the pitch between the baffles in the heat exchanger tends to increase the chances of turbulent flow on the side of the annulus. This, in turn, strengthens the impingement effects due to a greater number of baffles being present. The number of baffles is a key element in boosting the system's heat transfer efficiency, playing a significant role in its overall functionality. Nonetheless, it's crucial to acknowledge that this improvement incurs a cost; a marked increase in pressure drop is a consequence of the denser baffle configuration. This situation leads to a reinforcing effect where the closeness of baffles induces more turbulence, which in turn augments impingement, thereby elevating the heat transfer efficiency. Although this boost in heat transfer is advantageous for the system's performance, it's vital to consider this benefit against the downside of an increased pressure drop, which may affect the system's overall efficiency and operation. Ultimately, fine-tuning the baffle

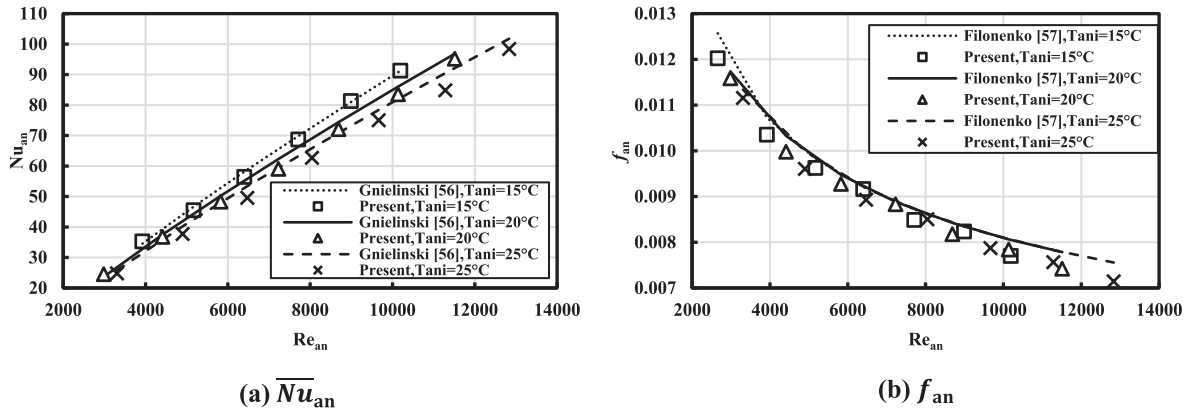
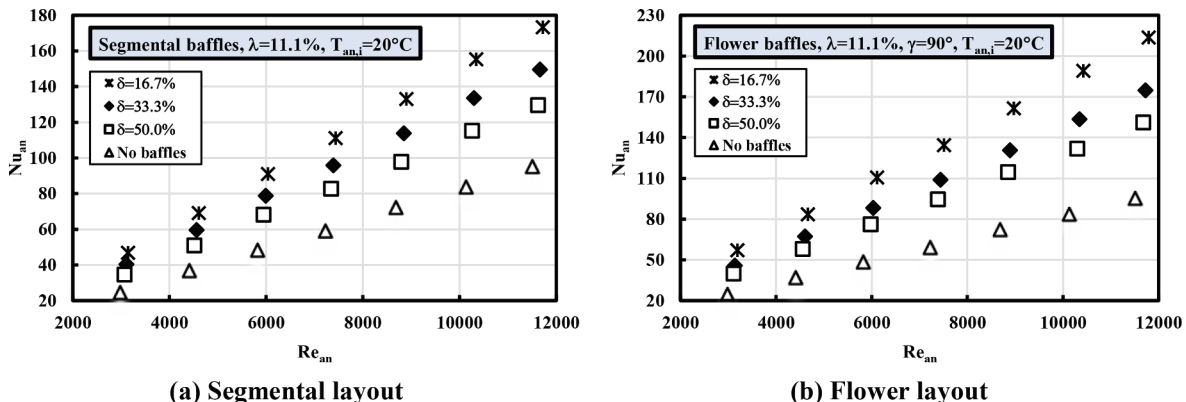
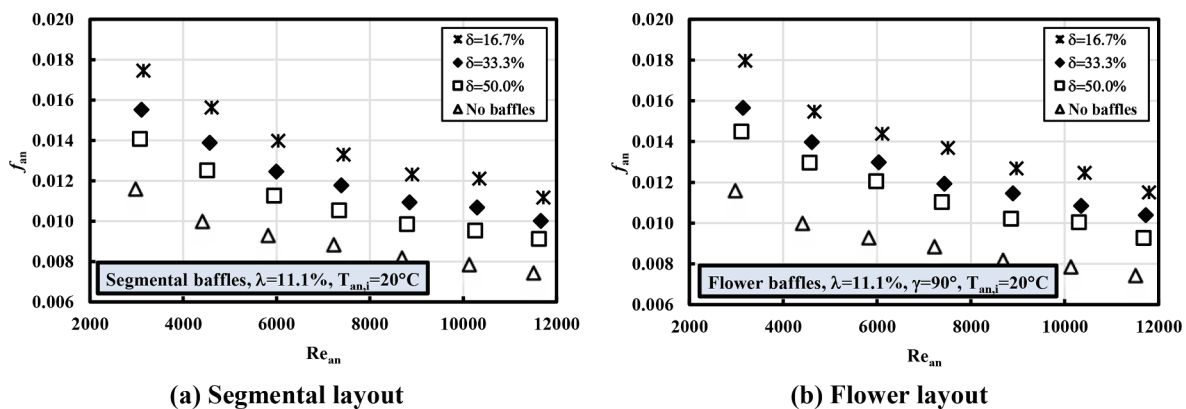


Fig. 5. Graphs of the validation results.

Fig. 6. Effect of baffle cut-off ratio on  $\overline{Nu}_{an}$ .Fig. 7. Effect of baffle cut-off ratio on  $f_{an}$ .

spacing to enhance heat transfer is a nuanced process that involves balancing the ideal conditions for turbulence and impingement against the resultant pressure drop.

### 7.3. Effect of the relative angle of the flower baffles

This analysis delves into the impact of the relative angle ( $\gamma$ ), which essentially denotes the angle formed by the centrelines of the cuts between successive flower baffles. The experimentation comprises runs that employ flower baffles designed for three distinct relative angles:  $30^\circ$ ,  $60^\circ$ , and  $90^\circ$ . These baffles are seamlessly integrated into the annular side of the heat exchanger, featuring a fixed cut-off ratio of 16.7

% and a pitch ratio of 11.1 %. The experimental procedures meticulously adhere to the specified operating conditions outlined in Table 2. Notably, Fig. 10 provides a representation of the results obtained for  $\overline{Nu}_{an}$  and  $f_{an}$  at an initial temperature level of  $T_{an,i} = 20^\circ\text{C}$ .

The findings from the study demonstrate a notable trend where the employment of baffles within the annular tube exerts a significant impact on both the Nusselt number and the coefficient of fluid friction. Specifically, as the relative angle of the baffles increases, so do the increases in these parameters. Comparing the scenarios with and without baffles, it is evident that the Nusselt number experiences considerable improvements, with average percentage increases of 119.5 %, 123.8 %, and 128.3 % observed at relative angles of  $30^\circ$ ,  $60^\circ$ , and  $90^\circ$ ,

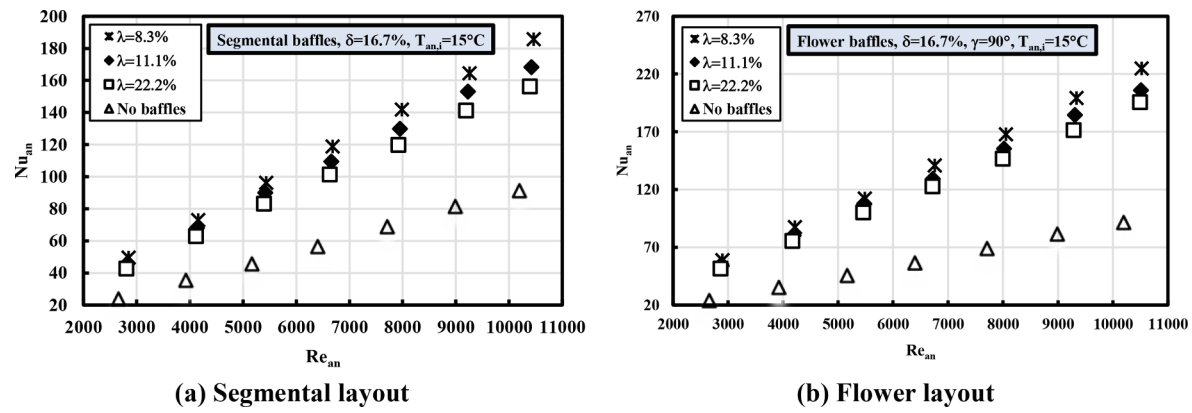
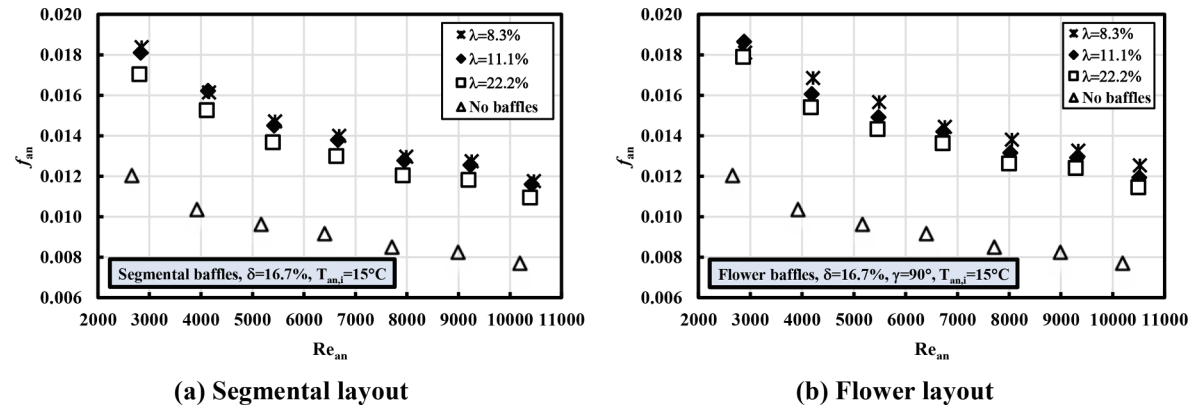
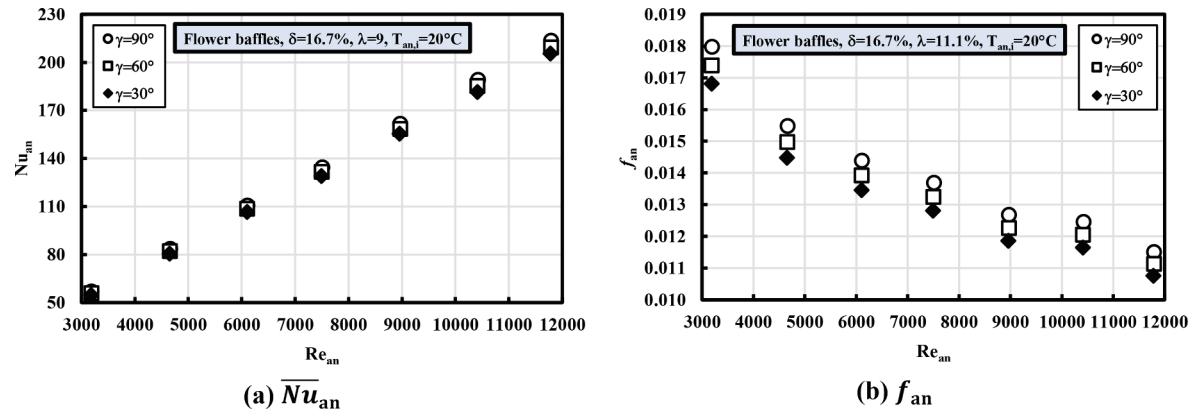
Fig. 8. Effect of baffle pitch ratio on  $\overline{Nu}_{an}$ .Fig. 9. Effect of baffle pitch ratio on  $f_{an}$ .

Fig. 10. Effect of baffle relative angle on heat exchanger performance.

respectively. Similarly, the coefficient of fluid friction also sees notable rises, registering increments of 45.8 %, 50.4 %, and 55.5 % at the corresponding relative angles.

Adjusting the relative angle of the baffle significantly enhances the mechanism's operational efficiency. This change not only alters the baffle's interaction with the fluid but also causes the fluid to stray from its original trajectory, leading to impacts against the outer surface of the inner tube. These alterations in flow patterns introduce a more intricate dynamic, marked by an increase in turbulence, the formation of eddies, and intensified mixing within the fluid's strata. Such disruptions have a considerable effect on the thermal boundary layer, leading to a significant improvement in the Nusselt number. Alongside this thermal

enhancement, there is a noticeable increase in pressure loss, particularly on the annular side, which underscores the complex balance of factors in play within this system. This detailed process of manipulation and the resulting series of events highlight the connection between geometric adjustments and their significant influence on flow and heat transfer properties, emphasizing the complex operation of this mechanism in a controlled setting.

#### 7.4. Effect of operating conditions in the annular pipe

In this analysis, a comprehensive examination is provided of how the varying operating conditions, specifically on the annulus side, affect the

performance parameters of the heat exchangers. Fig. 11 serves as a representation showcasing a sample of results derived, focusing on the flower baffle design with given parameters ( $\delta = 16.7\%$ ,  $\lambda = 8.3\%$ ,  $\gamma = 90^\circ$ ) for both the  $\overline{Nu}_{an}$  and  $f_{an}$  in relation to the annulus side inlet temperature changes across different flow rates.

The experimental findings demonstrate an obvious reduction in the  $\overline{Nu}_{an}$  as the temperature of the incoming water in the annulus increases. This trend is primarily attributed to the decline in the Prandtl number, which is a consequence of elevated water temperatures. Additionally, the results suggest that the temperature's impact on the friction factor in the annular tube is minimal, due to the predominance of the inertial forces over the viscosity variations induced by temperature shifts. Moreover, an increase in the  $Re_{an}$  contributes to higher Nusselt numbers, facilitated by the enhanced mixing of fluid layers and increased fluctuations over the internal tube surface. Conversely, with the rise of  $Re_{an}$ , the momentum forces begin to surpass the viscous forces, leading to a reduction in the friction factor.

### 7.5. Flower baffles versus conventional segmental baffles

The results reported in this study confirm that the heat transfer rate in the heat exchanger improves with the use of baffles while reducing both the cut-off and the pitch ratios (whether a traditional baffle or flower design is used). In addition, the heat transfer rate improves by increasing the relative angle of the flower-design baffles. However, these improvements in heat rate are accompanied by significant increases in pumping power required to overcome the increase in pressure loss in the annular tube fluid. Fig. 12 shows a sample of these results at an inlet temperature of  $15^\circ C$ , using conventional or flower design ( $\gamma = 90^\circ$ ) baffles, both with a cut-off ratio of  $16.7\%$  and at several pitch ratios from  $8.3\%$  to  $22.2\%$ . By inserting the baffles of  $\delta = 16.7\%$  and  $\lambda = 8.3\%$ , the findings report that the maximum enhancements in the  $\overline{Nu}_{an}$ , when compared with no baffles, are obtained as  $147.4\%$  and  $104.8\%$  with flower ( $\gamma = 90^\circ$ ) and segmental layouts, respectively. These conditions also coincide with the largest magnitude increases of  $60.2\%$  and  $53.7\%$ , respectively, in the annulus-friction factor. On average, the flower-design baffles achieve a higher Nusselt number in the annular tube than those using conventional segmental baffles, by an average increase of  $20.8\%$ , but this is associated with an increase in the coefficient of friction by an average of  $4.3\%$ . The improved performance of the flower-shaped baffles can be attributed to their unique design, which effectively reduces the wake zone behind them. In contrast, conventional single-segmental baffles, where the cut is made on one edge, tend to create a larger wake zone. This larger wake zone results in slower mixing between fluid layers around the internal tube. This is supported by the numerical simulations conducted by Sahel [45], which demonstrate that incorporating flower layout enhances flow mixing and disrupts areas of stagnation behind the baffles.

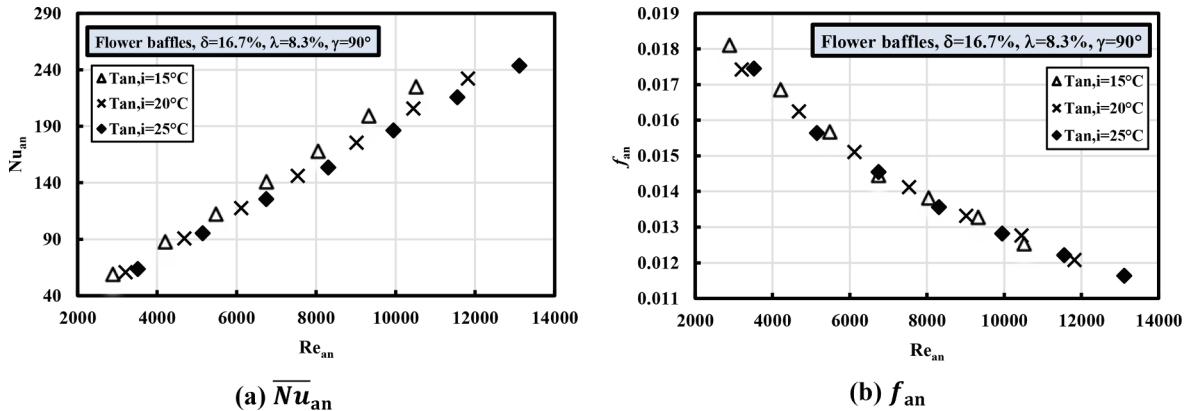


Fig. 11. Influence of annulus-side operating conditions on heat exchanger performance.

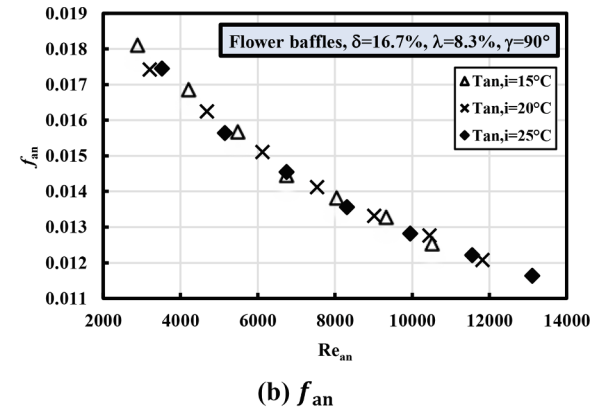
Now, the proposed technique for increasing heat exchange requires assessing if the convective heat transfer enhancement from baffles outweighs the increase in fluid flow pumping power. This comparison is crucial for evaluating the overall efficiency of heat exchangers with and without baffles. The combined Hydrothermal Performance Index ( $HTPI$ ) is calculated via Eq. (20) by analyzing the  $St_{an}$  and  $f_{an}$  ratios [2,58], providing insights into the capabilities and effectiveness of different heat exchanger configurations in facilitating efficient heat transfer processes. Eq. (20) is employed in this research due to the ability of the Stanton number ( $St = \overline{Nu}/RePr$ ) to integrate the disparities in the Reynolds and Prandtl numbers at the same flow rate during the various experiments. These discrepancies are attributed to the varying rates of heat transfer and the distinct thermophysical characteristics of the working fluid. Such an approach grants an equitable evaluation of the heat exchanger's hydrothermal efficacy across varied operational scenarios.

$$HTPI = \frac{St_{an, \text{baffle}}/St_{an, \text{no baffle}}}{(f_{an, \text{baffle}}/f_{an, \text{no baffle}})^{1/3}} \quad (20)$$

For various baffle cut-off, pitch ratios, relative angles, and annulus-side working circumstances, the  $HTPI$  is evaluated, and samples of the outputs are documented in Fig. 13. For all ranges of the parameters under investigation,  $HTPI$  is greater than unity. Furthermore, compared to the traditional segmental layout, the suggested flower-design baffles perform better. Additionally, the  $HTPI$  is enhanced by increasing the baffle relative angle while decreasing with increasing baffle cut-off and pitch ratios, annulus-side Reynolds, and Prandtl numbers. The results show that the highest  $HTPI$  recorded is 2.23, which is achieved by operating the annular pipe at the lowest flow rate and water inlet temperature, along with incorporating flower baffles characterized by specific dimensions of  $\delta = 16.7\%$ ,  $\lambda = 8.3\%$ , and  $\gamma = 90^\circ$ . Employing traditional segmental baffles under the same operating conditions results in an  $HTPI$  value of 1.85. These findings underscore the significant impact of baffle design and operational parameters on heat transfer performance in the heat exchanger. In Fig. 14, the highest  $HTPI$  in this study (2.23), is compared analytically to indices published by researchers working on double-tube heat exchangers and using different augmentation techniques. This comparison study highlights how the design shown here is superior to others in the field and is in line with the state of the art in research. The effectiveness of the unique "floral baffle" arrangement in increasing thermal efficiency is further supported by this evidence.

## 8. Correlations

In the current investigational data provided, sets of correlations are established to predict key parameters such as  $\overline{Nu}_{an}$ ,  $f_{an}$ , and  $HTPI$  for the



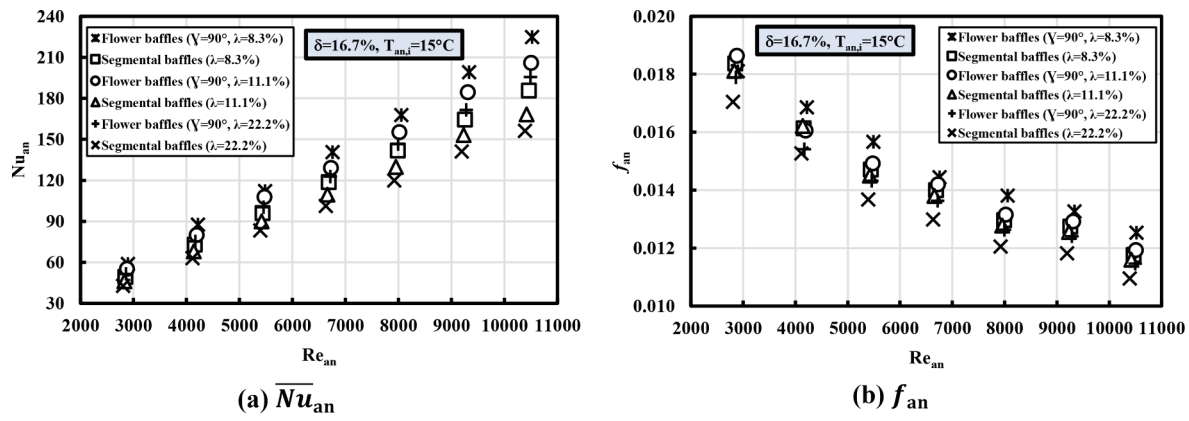


Fig. 12. Effect of baffle layout on the heat exchanger performance.

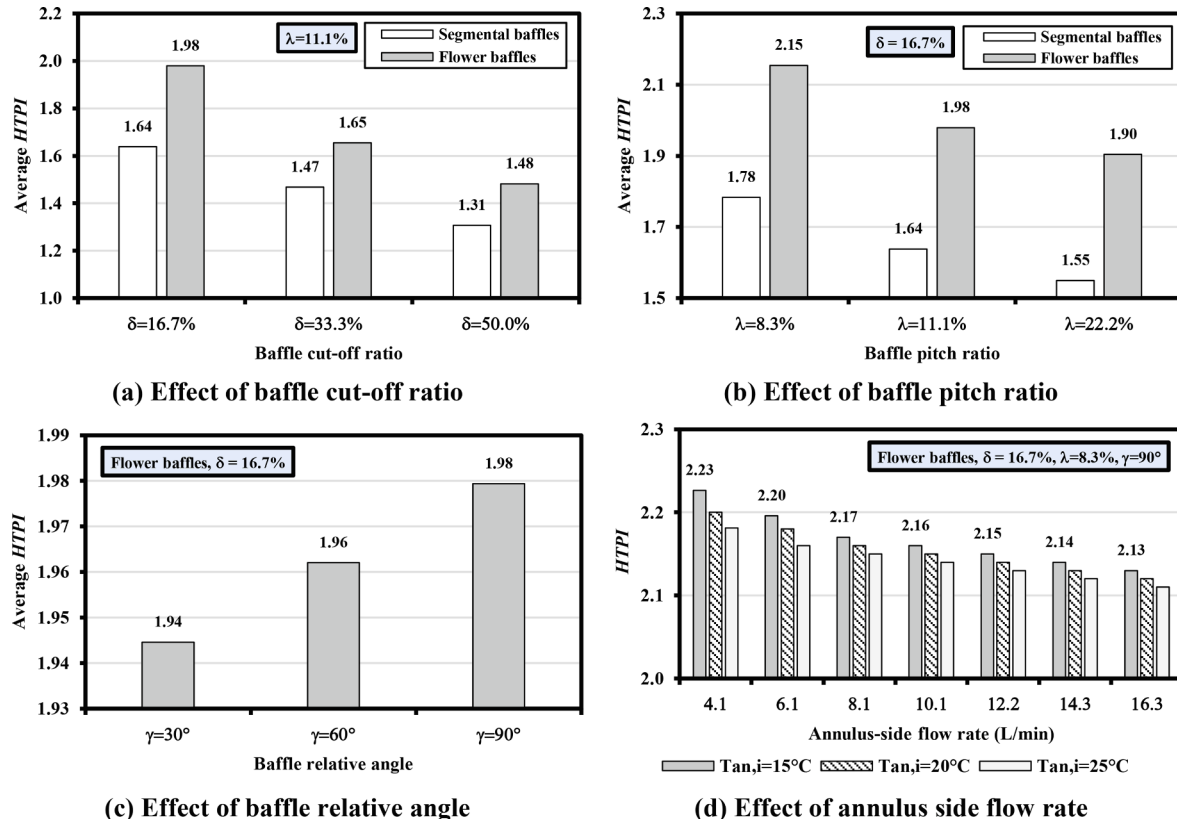


Fig. 13. The average HTPI of the heat exchanger.

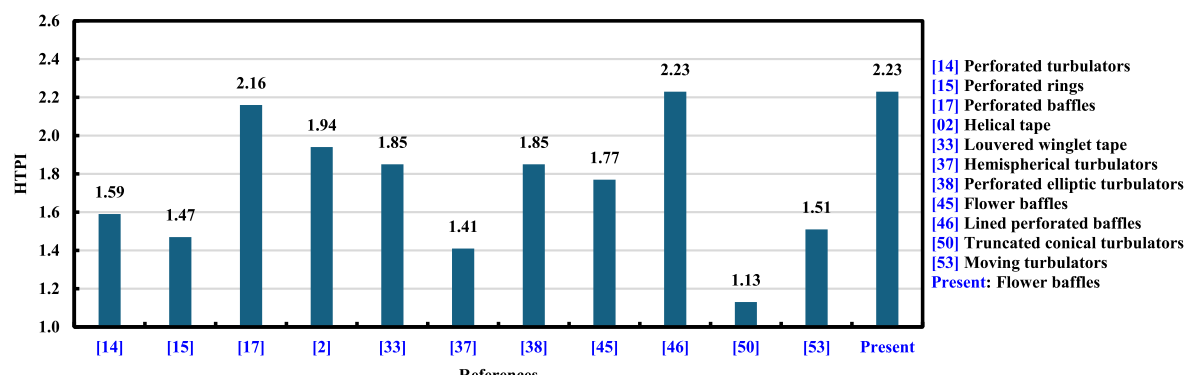


Fig. 14. The HTPI of double pipe heat exchangers in present and other published studies.

- [14] Perforated turbulators
- [15] Perforated rings
- [17] Perforated baffles
- [02] Helical tape
- [33] Louvered winglet tape
- [37] Hemispherical turbulators
- [38] Perforated elliptic turbulators
- [45] Flower baffles
- [46] Lined perforated baffles
- [50] Truncated conical turbulators
- [53] Moving turbulators
- Present: Flower baffles

two different baffle designs under consideration. Specifically, for the conventional segmental baffle, the correlations (Eqs. (21) to (23)) are applicable within the ranges of  $2660 \leq Re_{an} \leq 13040$ ,  $5.28 \leq Pr_{an} \leq 7.48$ ,  $16.7\% \leq \delta \leq 50\%$ , and  $8.3\% \leq \lambda \leq 22.2\%$ . On the other hand, for the flower-design baffle, the correlations (Eqs. (24) to (26)) are valid for the ranges of  $2660 \leq Re_{an} \leq 13110$ ,  $5.21 \leq Pr_{an} \leq 7.48$ ,  $16.7\% \leq \delta \leq 50\%$ ,  $8.3\% \leq \lambda \leq 22.2\%$ , as well as  $30^\circ \leq \gamma \leq 90^\circ$ . Furthermore, it is important to note that all correlations of  $\bar{Nu}_{an}$  and  $f_{an}$  remain applicable for double pipe heat exchangers without baffles, provided that the conditions  $\delta = \lambda = 1$  and  $\gamma = 0$  are satisfied across the system. The comprehensive analysis of these correlations aids in understanding and predicting heat transfer performance for the given baffle designs and further extends the applicability to similar systems in the absence of baffles. With maximum variances of  $\pm 6.9\%$ ,  $\pm 6.3\%$ , and  $\pm 4.8\%$  for  $\bar{Nu}_{an}$ ,  $HTPI$ , and  $f_{an}$ , respectively, the suggested correlations anticipate the current experimental findings as demonstrated in Figs. 15 and 16.

For conventional segmental baffles, the proposed correlations are:

$$\bar{Nu}_{an} = 0.0036 Re_{an}^{0.9686} Pr_{an}^{0.5875} \delta^{-0.254} \lambda^{-0.0903} \quad (21)$$

$$f_{an} = 0.1568 Re_{an}^{-0.3265} \delta^{-0.1783} \lambda^{-0.0488} \quad (22)$$

$$HTPI = 1.205 Re_{an}^{-0.0326} Pr_{an}^{-0.0390} \delta^{-0.2250} \lambda^{-0.1334} \quad (23)$$

For flower baffles, the proposed correlations are:

$$\bar{Nu}_{an} = 0.0036 Re_{an}^{0.9837} Pr_{an}^{0.5148} \delta^{-0.3211} \lambda^{-0.0850} \left(1 + \frac{\gamma}{360}\right)^{0.3215} \quad (24)$$

$$f_{an} = 0.146 Re_{an}^{-0.3186} \delta^{-0.1726} \lambda^{-0.0324} \left(1 + \frac{\gamma}{360}\right)^{0.3530} \quad (25)$$

$$HTPI = 1.148 Re_{an}^{-0.0220} Pr_{an}^{-0.0440} \delta^{-0.2931} \lambda^{-0.1098} \left(1 + \frac{\gamma}{360}\right)^{0.3712} \quad (26)$$

## 9. Conclusions

This research experimentally investigates the hydrothermal behavior

of a horizontal double-pipe heat exchanger with counter-flow arrangement, utilizing standard segmental baffles and innovative flower-patterned baffles within the annular space. The key variables examined are the baffles' relative angle, cut-off, and pitch ratios, and the annular side's operational conditions. During the tests, hot water at  $70^\circ C$  flows at a constant flow rate in the internal tube while cold water flows in the annular pipe within the ranges of  $2660 \leq Re_{an} \leq 13110$ ,  $5.21 \leq Pr_{an} \leq 7.48$ . The baffles are of geometry specifications of  $16.7\% \leq \delta \leq 50\%$ , and  $8.3\% \leq \lambda \leq 22.2\%$ . Besides, the flower design has a relative angle between  $30^\circ$  and  $90^\circ$ . The key findings are summarized as follows:

- The  $\bar{Nu}_{an}$  and  $f_{an}$  increase significantly when baffles are inserted in the annular side of the heat exchanger. This effect holds true whether conventional baffles or the suggested flower design are used. Lowering the baffle's cut-off and pitch ratios further raises these increases.
- By incorporating baffles with dimensions  $\delta = 16.7\%$  and  $\lambda = 8.3\%$ , significant enhancements in the  $\bar{Nu}_{an}$  are observed compared to cases without baffles. Specifically:
  - With flower baffles ( $\gamma = 90^\circ$ ), the maximum enhancement is 147.4 %.
  - With segmental layouts, the maximum enhancement is 104.8 %.
- These conditions also corresponded to substantial increases in the annulus-friction factor: 60.2 % and 53.7 %, respectively.
- Raising the relative angle of the flower baffles increases  $\bar{Nu}_{an}$  but also raises the annular pipe's pressure loss.
- Interestingly, the temperature does not impact the friction factor, but it significantly reduces  $\bar{Nu}_{an}$  with rising annulus-fluid inlet temperature.
- Increasing the  $Re_{an}$  results in higher Nusselt numbers and a lower friction factor.
- On average, flower-design baffles improve the  $\bar{Nu}_{an}$  by 20.8 % more than conventional segmental baffles. However, this improvement comes at the cost of a 4.3 % increase in the coefficient of friction.

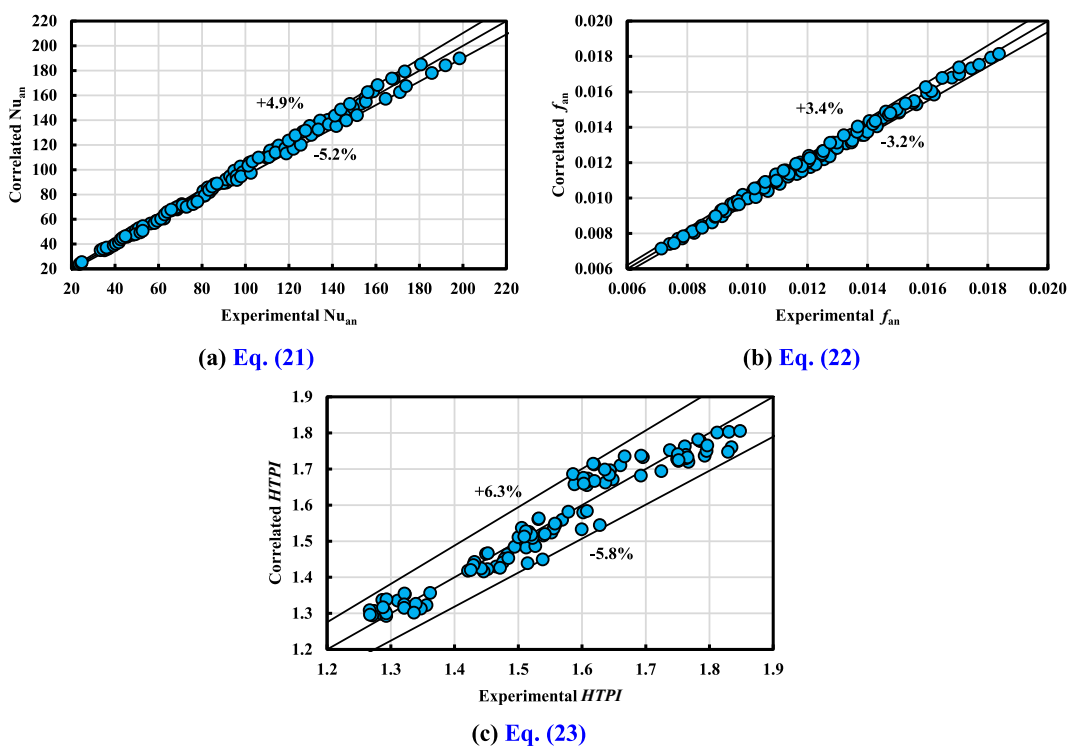


**Fig. 15.** Comparisons between the correlated outputs and the current experimental results for conventional segmental baffles.

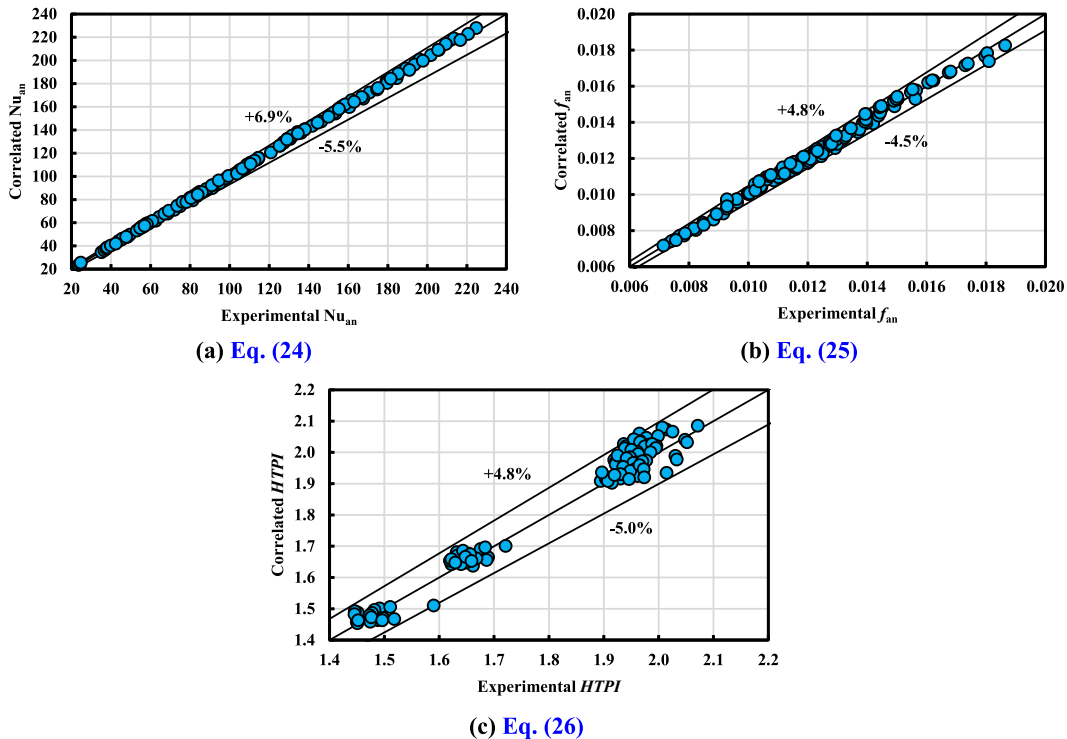


**Fig. 16.** Comparisons between the correlated outputs and the current experimental results for flower baffles.

- The temperature of the working fluid does not affect the friction factor, while the  $\bar{N}\!u_{an}$  significantly reduces with rising annulus-fluid inlet temperature.
- The HTPI is evaluated to assess the heat exchanger's performance with baffles. Across parameter ranges:
  - HTPI consistently exceeds unity.
  - Flower-design baffles outperform the conventional segmental layout.
  - HTPI decreases with increasing annulus-side Reynolds and Prandtl numbers, baffle cut-off, and pitch ratios.
  - The maximum recorded HTPI (2.23) occurs with specific flower baffle specifications ( $\delta = 16.7\%$ ,  $\lambda = 8.3\%$ ,  $\gamma = 90^\circ$ ).

- Experimental correlations for  $\bar{N}\!u_{an}$ , HTPI, and  $f_{an}$  predictions are suggested.

#### Declaration of competing interest

The authors declare that they have no known competing financial interests or personal relationships that could have appeared to influence the work reported in this paper.

#### Data availability

Data will be made available on request.

## Appendix A

As suggested by Kline and McClintock [55], the impacts of every variable are considered to assess the uncertainty in the computed parameters:

$$\frac{\omega_\delta}{\delta} = \pm \sqrt{\left(\frac{\omega_{A_{cut}}}{A_{cut}}\right)^2 + \left(\frac{2\omega_{d_{an}}}{d_{an}}\right)^2} = \pm \sqrt{\left(\frac{0.1}{100}\right)^2 + \left(\frac{2x0.05}{56}\right)^2} = \pm 0.2\% \quad (\text{A.1})$$

$$\frac{\omega_\lambda}{\lambda} = \pm \sqrt{\left(\frac{\omega_{p_{baffle}}}{p_{baffle}}\right)^2 + \left(\frac{\omega_{L_t}}{L_t}\right)^2} = \pm \sqrt{\left(\frac{0.5}{150}\right)^2 + \left(\frac{0.5}{1800}\right)^2} = \pm 0.33\% (\text{Max.}) \quad (\text{A.2})$$

$$\omega_{\Delta T} = \pm \sqrt{(\omega_{T_i})^2 + (\omega_{T_o})^2} = \pm \sqrt{2(0.5)^2} = \pm 0.71^\circ\text{C} \quad (\text{A.3})$$

$$\omega_{\Delta T_{LM}} = \pm \frac{\omega_T \sqrt{2}}{\ln \left[ \frac{\Delta T_1}{\Delta T_2} \right]} \sqrt{2 - 2\Delta T_{LM} \left( \frac{1}{\Delta T_1} + \frac{1}{\Delta T_2} \right) + \Delta T_{LM}^2 \left( \frac{1}{\Delta T_1^2} + \frac{1}{\Delta T_2^2} \right)} = \pm 0.5^\circ\text{C} (\text{Max.}) \quad (\text{A.4})$$

$$\omega_{\dot{V}} = \pm \sqrt{\left(\frac{\omega_V}{t}\right)^2 + \left(\frac{-V}{t^2} \omega_t\right)^2} = \pm \sqrt{\left(\frac{1}{1} x 0.01\right)^2 + \left(\frac{-20}{1^2} x \left(\frac{1}{60}\right)\right)^2} = \pm 1.67\% \quad (\text{A.5})$$

$$\frac{\omega_{\dot{m}_t}}{\dot{m}_t} = \pm \sqrt{\left(\frac{\omega_{\rho_t}}{\rho_t}\right)^2 + \left(\frac{\omega_{V_t}}{V_t}\right)^2} = \pm \sqrt{\left(\frac{0.1}{100}\right)^2 + \left(\frac{1.67}{100}\right)^2} = \pm 1.67\% \quad (\text{A.6})$$

$$\frac{\omega_{Re_t}}{Re_t} = \pm \sqrt{\left(\frac{\omega_{\dot{m}_t}}{\dot{m}_t}\right)^2 + \left(\frac{-\omega_{d_{t,i}}}{d_{t,i}}\right)^2 + \left(\frac{-\omega_{\mu_t}}{\mu_t}\right)^2} = \pm 1.69\% \quad (\text{A.7})$$

$$\omega_{d_{an,h}} = \pm \sqrt{(\omega_{d_{an,i}})^2 + (\omega_{d_{t,o}})^2} = \pm \sqrt{(0.5)^2 + (0.05)^2} = \pm 0.5\text{mm} \quad (\text{A.8})$$

$$\frac{\omega_{Re_{an}}}{Re_{an}} = \pm \sqrt{\left(\frac{\omega_{\dot{m}_{an}}}{\dot{m}_{an}}\right)^2 + \left(\frac{-\omega_{d_{an,h}}}{d_{an,h}}\right)^2 + \left(\frac{-\omega_{\mu_{an}}}{\mu_{an}}\right)^2} = \pm 1.91\% \quad (\text{A.9})$$

$$\frac{\omega_{Q_t}}{Q_t} = \pm \sqrt{\left(\frac{\omega_{\dot{m}_t}}{\dot{m}_t}\right)^2 + \left(\frac{\omega_{Cp_t}}{Cp_t}\right)^2 + \left(\frac{\omega_{\Delta T_t}}{\Delta T_t}\right)^2} = \pm 5.57\% \quad (\text{A.10})$$

$$\frac{\omega_{Q_{an}}}{Q_{an}} = \pm \sqrt{\left(\frac{\omega_{\dot{m}_{an}}}{\dot{m}_{an}}\right)^2 + \left(\frac{\omega_{Cp_{an}}}{Cp_{an}}\right)^2 + \left(\frac{\omega_{\Delta T_{an}}}{\Delta T_{an}}\right)^2} = \pm 6.34\% \quad (\text{A.11})$$

$$\omega_{Q_{ave}} = \pm \frac{1}{2} \sqrt{(\omega_{Q_t})^2 + (\omega_{Q_{an}})^2} = \pm 4.22\% \quad (\text{A.12})$$

$$\frac{\omega_{\bar{N}u_t}}{\bar{N}u_t} = \pm \sqrt{\left(\frac{0.8\omega_{Re_t}}{Re_t}\right)^2 + \left(\frac{0.4\omega_{Pr_t}}{Pr_t}\right)^2} = \pm 1.35\% \quad (\text{A.13})$$

$$\frac{\omega_{\bar{h}_t}}{\bar{h}_t} = \pm \sqrt{\left(\frac{\omega_{\bar{N}u_t}}{\bar{N}u_t}\right)^2 + \left(\frac{\omega_{k_t}}{k_t}\right)^2 + \left(\frac{-\omega_{d_{t,i}}}{d_{t,i}}\right)^2} = \pm 1.71\% \quad (\text{A.14})$$

$$\frac{\omega_{A_{t,i}}}{A_{t,i}} = \frac{\omega_{A_{t,o}}}{A_{t,o}} = \pm \sqrt{\left(\frac{\omega_{d_{t,i}}}{d_{t,i}}\right)^2 + \left(\frac{\omega_{L_t}}{L_t}\right)^2} = \pm 0.23\% \quad (\text{A.15})$$

$$\frac{\omega_{U_i}}{U_i} = \pm \sqrt{\left(\frac{\omega_{Q_{ave}}}{Q_{ave}}\right)^2 + \left(\frac{-\omega_{A_{t,i}}}{A_{t,i}}\right)^2 + \left(\frac{-\omega_{\Delta T_{LM}}}{\Delta T_{LM}}\right)^2} = \pm 4.46\% \quad (\text{A.16})$$

$$\omega_{\bar{h}_{an}} = \pm \sqrt{\left(\frac{\partial \bar{h}_{an}}{\partial U_i} \omega_{U_i}\right)^2 + \left(\frac{\partial \bar{h}_{an}}{\partial A_{t,o}} \omega_{A_{t,o}}\right)^2 + \left(\frac{\partial \bar{h}_{an}}{\partial A_{t,i}} \omega_{A_{t,i}}\right)^2 + \left(\frac{\partial \bar{h}_{an}}{\partial \bar{h}_t} \omega_{\bar{h}_t}\right)^2} = \pm 3.02\% \quad (\text{A.17})$$

$$\frac{\omega_{\bar{N}u_{an}}}{\bar{N}u_{an}} = \pm \sqrt{\left(\frac{\omega_{\bar{h}_{an}}}{\bar{h}_{an}}\right)^2 + \left(\frac{\omega_{d_{an,h}}}{d_{an,h}}\right)^2 + \left(\frac{-\omega_{k_{an}}}{k_{an}}\right)^2} = \pm 3.15\% \quad (\text{A.18})$$

$$\frac{\omega_{St_{an}}}{St_{an}} = \pm \sqrt{\left(\frac{\omega_{\bar{N}u_{an}}}{\bar{N}u_{an}}\right)^2 + \left(\frac{\omega_{Re_{an}}}{Re_{an}}\right)^2 + \left(\frac{\omega_{Pr_{an}}}{Pr_{an}}\right)^2} = \pm 3.69\% \quad (\text{A.19})$$

$$\frac{\omega_{f_{an}}}{f_{an}} = \pm \sqrt{\left(\frac{\omega_{\Delta P_{an}}}{\Delta P_{an}}\right)^2 + \left(\frac{5\omega_{d_{sh,h}}}{d_{an,h}}\right)^2 + \left(\frac{\omega_{\rho_{an}}}{\rho_{an}}\right)^2 + \left(\frac{-\omega_{L_{an}}}{L_{an}}\right)^2 + \left(\frac{-2\omega_{\dot{m}_{an}}}{\dot{m}_{an}}\right)^2} = \pm 5.67\% \quad (\text{A.20})$$

$$\frac{\omega_{HTPI}}{HTPI} = \pm \sqrt{\left(\frac{\omega_{St_{an,baffle}}}{St_{an,baffle}}\right)^2 + \left(\frac{\omega_{St_{an,no baffle}}}{St_{an,no baffle}}\right)^2 + \left(\frac{\frac{1}{3}\omega_{f_{an,baffle}}}{f_{an,baffle}}\right)^2 + \left(\frac{\frac{1}{3}\omega_{f_{an,no baffle}}}{f_{an,no baffle}}\right)^2} = \pm 5.9\% \quad (\text{A.21})$$

## References

- [1] S. Al-Zahrani, Heat transfer characteristics of innovative configurations of double pipe heat exchanger, *Heat Mass Transf.* 59 (2023) 1661–1675.
- [2] M.R. Salem, M. Eltoukhey, R. Ali, K. Elshazly, Experimental investigation on the hydrothermal performance of a double-pipe heat exchanger using helical tape insert, *Int. J. Therm. Sci.* 124 (2018) 496–507.
- [3] M.H. Mousa, N. Miljkovic, K. Nawaz, Review of heat transfer enhancement techniques for single phase flows, *Renewable Sustainable Energy Rev.* 137 (2021) 110566.

- [4] N.M. Almulla, M.A. Moawed, M.A. Abd Elrahman, M.R. Salem, Effect of baffle configuration on the thermal performance attributes of shell and semi-circular tube heat exchangers, Eng. Res. J. (shoubra) 53 (1) (2024) 279–291.
- [5] Y. Lei, Y. He, P. Chu, R. Li, Design and optimization of heat exchangers with helical baffles, Chem. Eng. Sci. 63 (2008) 4386–4395.
- [6] J. Zhang, S. Guo, Z. Li, J. Wang, Y. He, W. Tao, Experimental performance comparison of shell-and-tube oil coolers with overlapped helical baffles and segmental baffles, Appl. Therm. Eng. 58 (1–2) (2013) 336–343.
- [7] N. Targui, H. Kahalerras, Analysis of a double pipe heat exchanger performance by use of porous baffles and pulsating flow, Energy Convers. Manag. 76 (2013) 43–54.
- [8] S.A. Hussein, Experimental investigation of double pipe heat exchanger by using semi circular disc baffles, Int. J. Comput. Appl. 115 (4) (2015) 13–17.
- [9] G. Zhou, J. Xiao, L. Zhu, J. Wang, S. Tu, A numerical study on the shell-side turbulent heat transfer enhancement of shell-and-tube heat exchanger with trefoil hole baffles, Energy Procedia 75 (2015) 3174–3179.
- [10] A. El Maakoul, A. Lakanizi, S. Saadeddine, M. El Metoui, A. Zaite, M. Meziane, A. Abdellah, Numerical comparison of shell-side performance for shell and tube heat exchangers with trefoil-hole, helical and segmental baffles, Appl. Therm. Eng. 109 (2016) 175–185.
- [11] X. Gu, B. Liu, Y. Wang, K. Wang, Heat Transfer and flow resistance performance of shutter baffle heat exchanger with triangle tube layout in shell side, Adv. Mech. Eng. 8 (3) (2016) 1–8.
- [12] A.S. Ambekar, R. Sivakumar, N. Anantharaman, M. Vivekenandan, CFD simulation study of shell and tube heat exchangers with different baffle segment configurations, Appl. Therm. Eng. 108 (2016) 999–1007.
- [13] P.S. Amirtharaj, S. Allaordinbasha, M. Janagan, R. Karthikeyan, S. Muthukumar, Design and analysis of shell and tube heat exchanger with inclined baffles, Int. J. Dev. Res. 1 (3) (2016) 252–260.
- [14] M. Sheikholeslami, D.D. Ganji, Heat transfer improvement in a double pipe heat exchanger by means of perforated turbulators, Energy Convers. Manag. 127 (2016) 112–123.
- [15] A. Kumar, S. Chamoli, M. Kumar, S. Singh, Experimental investigation on thermal performance and fluid flow characteristics in circular cylindrical tube with circular perforated ring inserts, Exp. Therm. Fluid Sci. 79 (2016) 168–174.
- [16] M. Mellat, R. Benzeguir, D. Sahel, H. Ameur, Hydro-thermal shell-side performance evaluation of a shell and tube heat exchanger under different baffle arrangement and orientation, Int. J. Therm. Sci. 121 (2017) 138–149.
- [17] M.R. Salem, M.K. Althaferi, K.M. Elshazly, M.G. Higazy, M.F. Abdabbo, Experimental investigation on the thermal performance of a double pipe heat exchanger with segmental perforated baffles, Int. J. Therm. Sci. 122 (2017) 39–52.
- [18] J. Wena, H. Yang, S. Wang, X. Gu, PIV Experimental investigation on shell-side flow patterns of shell and tube heat exchanger with different helical baffles, Int. J. Heat Mass Transf. 104 (2017) 247–259.
- [19] X. Zhang, D. Han, W. He, C. Yue, W. Pu, Numerical simulation on a novel shell-and-tube heat exchanger with screw cinquefoil orifice baffles, Adv. Mech. Eng. 9 (2017) 1–12.
- [20] P. Bichkar, O. Dandgaval, P. Dalvi, R. Godase, T. Dey, Study of shell and tube heat exchanger with the effect of types of baffles, Procedia Manuf. 20 (2018) 195–200.
- [21] A.B. Colaço, F. Bernardo, M.B. Lopes, V.C. Mariani, L. Coelho, M.R. Salem, Optimization of double pipe-heat exchanger with single segmental perforated baffles, 17<sup>th</sup> Brazilian Congress of Thermal Sciences and Engineering, November 25<sup>th</sup>-28<sup>th</sup>, 2018, Águas de Lindóia, SP, Brazil), 234, 0234.
- [22] R. Amini, M. Amini, A. Jafarinia, M. Kashfi, Numerical investigation on effects of using segmented and helical tube fins on thermal performance and efficiency of a shell and tube heat exchanger, Appl. Therm. Eng. 138 (2018) 750–760.
- [23] X. Wang, N. Zheng, Z. Liu, W. Liu, Numerical analysis and optimization study on shell-side performances of a shell and tube heat exchanger with staggered baffles, Int. J. Heat Mass Transf. 124 (2018) 247–259.
- [24] M.O. Petrinir, A.A. Dare, Numerical investigation of the concave-cut baffles effect in shell-and-tube heat exchanger, J. Eng. Sci. 6 (1) (2019) 1–9.
- [25] R.K. Ajeel, W.S.I.W. Salim, K. Hasnan, Influences of geometrical parameters on the heat transfer characteristics through symmetry trapezoidal-corrugated channel using SiO<sub>2</sub>-water nanofluid, Int. Commun. Heat Mass Transf. 101 (2019) 1–9.
- [26] R.K. Ajeel, W.S.I.W. Salim, K. Hasnan, Design characteristics of symmetrical semicircle-corrugated channel on heat transfer enhancement with nanofluid, Int. J. Mech. Sci. 151 (2019) 236–250.
- [27] R.K. Ajeel, W.S.I.W. Salim, K. Hasnan, Experimental and numerical investigations of convection heat transfer in corrugated channels using alumina nanofluid under a turbulent flow regime, Chem. Eng. Res. Des. 148 (2019) 202–217.
- [28] R.K. Ajeel, W.S.I.W. Salim, K. Sopian, M.Z. Yusoff, K. Hasnan, A. Ibrahim, A.H. Al-Waeli, Turbulent convective heat transfer of silica oxide nanofluid through corrugated channels: An experimental and numerical study, Int. J. Heat Mass Transf. 145 (2019) 118806.
- [29] R.K. Ajeel, W.S.I.W. Salim, K. Hasnan, Comparative study of the thermal performance of corrugated channels using ZnO–water nanofluid, J. Thermophys. Heat Transfer 33 (2) (2019) 508–516.
- [30] R.K. Ajeel, W.S.I.W. Salim, K. Sopian, M.Z. Yusoff, Analysis of thermal-hydraulic performance and flow structures of nanofluids across various corrugated channels: An experimental and numerical study, Therm. Sci. Eng. Prog. 19 (2020) 100604.
- [31] R.K. Ajeel, W.S.I.W. Salim, Combined effects of nanofluid and geometrical structures of a parallel plate channel with semicircle corrugations on flow characteristics and thermal-hydraulic performance, J. Thermal Sci. Eng. Appl. 12 (4) (2020) 041025.
- [32] R.K. Ajeel, W.S.I.W. Salim, Experimental assessment of heat transfer and pressure drop of nanofluid as a coolant in corrugated channels, J. Therm. Anal. Calorim. 144 (2021) 1161–1173.
- [33] R. Thejaraju, K.B. Girisha, S.H. Manjunath, B.S. Dayananda, Numerical evaluation of thermo-hydraulic performance index of a double pipe heat exchanger using double sided louvered winglet tape, J. Therm. Eng. 6 (5) (2020) 843–857.
- [34] C. Bensaci, A. Moummi, F. Flor, E. Jara, A. Rincon-Casado, A. Ruiz-Pardo, Numerical and experimental study of the heat transfer and hydraulic performance of solar air heaters with different baffle positions, Renew. Energy 155 (C) (2020) 1231–1244.
- [35] M.H. Mohammadi, H.R. Abbasi, A. Yavarinasab, H. Pourrahmani, Thermal optimization of shell and tube heat exchanger using porous baffles, Appl. Therm. Eng. 170 (2020) 115005.
- [36] J. Mahendran, Experimental analysis of shell and tube heat exchanger using flower baffle plate configuration, Mater. Today: Proc. 21 (Part 1) (2020) 419–424.
- [37] S. Kumar, P. Dinesha, A. Narayanan, R. Nanda, Effect of hemispherical turbulators in a double pipe heat exchanger for heat transfer augmentation, J. Turbul. 21 (3) (2020) 166–185.
- [38] M.E. Nakhchi, M. Hatami, M. Rahmati, Experimental investigation of performance improvement of double-pipe heat exchangers with novel perforated elliptic turbulators, Int. J. Therm. Sci. 168 (2021) 107057.
- [39] A. Youcef, R. Saim, Numerical analysis of the baffles inclination on fluid behavior in a shell and tube heat exchanger, J. Appl. Comput. Mech. 7 (1) (2021) 312–320.
- [40] S. Gaikwad, A. Parmar, Numerical simulation of the effect of baffle cut and baffle spacing on shell side heat exchanger performance using CFD, Chem. Prod. Process Model. 16 (2) (2021) 145–154.
- [41] J. Chen, P. Zhao, Q. Wang, M. Zeng, Experimental investigation of shell-side performance and optimal design of shell-and-tube heat exchanger with different flower baffles, Heat Transf. Eng. 42 (7) (2021) 613–626.
- [42] R.K. Ajeel, K. Sopian, R. Zulkifli, A novel curved-corrugated channel model: Thermal-hydraulic performance and design parameters with nanofluid, Int. Commun. Heat Mass Transf. 120 (2021) 105037.
- [43] R.K. Ajeel, K. Sopian, R. Zulkifli, Thermal-hydraulic performance and design parameters in a curved-corrugated channel with L-shaped baffles and nanofluid, J. Energy Storage 34 (2021) 101996.
- [44] R.K. Ajeel, R. Zulkifli, K. Sopian, S.N. Fayyadh, A. Fazlizan, A. Ibrahim, Powder Technol. 385 (2021) 144–159.
- [45] D. Sahel, Thermal performance assessment of a tubular heat exchanger fitted with flower baffles, J. Thermophys. Heat Transf. 35 (4) (2021) 726–734.
- [46] A. Colaço, V.C. Mariani, M.R. Salem, L. Coelho, Maximizing the thermal performance index applying evolutionary multi-objective optimization approaches for double pipe heat exchanger, Appl. Therm. Eng. 211 (2022) 118504.
- [47] A. Kalera, S. Venkatesh, N. Kumar, Numerical and experimental study of a shell and tube heat exchanger for different baffles, Heat Transf. 52 (3) (2022) 2186–2206.
- [48] M. Saad, A. Munir, M.A. Kamran, Numerical simulations of shell and tube heat exchanger with segmental, trefoil and segmented trefoil baffles for performance comparison, Heat Transf. Eng. 44 (8) (2023) 702–719.
- [49] P. Samruaisin, R. Maza, C. Thianpong, V. Chuwattanakul, N. Maruyama, M. Hirota, S. Eiamsa-ard, Enhanced heat transfer of a heat exchanger tube installed with V-shaped delta-wing baffle turbulators, Energies 16 (13) (2023) 5237.
- [50] S. Kumar, H. Girish, A. Ganesh, N. Kumar, Enhancement in heat transfer characteristics by using truncated conical turbulators in a double pipe heat exchanger under turbulent conditions, Cogent. Eng. 10 (2023) 2250069.
- [51] J. Ji, Y. Pan, J. Zhang, B. Shi, L. Bao, Numerical study on the effect of baffle structure on the heat transfer performance of elastic tube bundle heat exchanger, Appl. Therm. Eng. 238 (2024) 122220.
- [52] N.M. Almulla, M.A. Moawed, M.A. Abd Elrahman, M.R. Salem, Study of the thermal performance characteristics of shell and semi-circular tube heat exchanger using both baffles and nanofluid, Eng. Res. J. (shoubra) 53 (2) (2024) 68–81.
- [53] S. Banihashemi, M. Assari, S. Javadi, S. Vahidifar, Study the effect of innovative active and passive methods on thermal characteristics and turbulent flow behaviour in a heat exchanger pipe, J. Therm. Anal. Calorim. 149 (2024) 777–797.
- [54] F.W. Dittus, L.M.K. Boelter, Heat transfer in automobile radiators of the tubular type, University of California Publications in Engineering, 1930, 2,443461. Lawrence, A. E.
- [55] S.J. Kline, F.A. McClintock, Describing uncertainties in single-sample experiments, Mech. Eng. 75 (1) (1953) 3–8.
- [56] V. Gnielinski, New equations for heat and mass transfer in turbulent pipe and channel flow, Int. Chem. Eng. 16 (1976) 359–368.
- [57] G.K. Filonenko, Hydraulic resistance of pipes (Hydraulischer widerstand von röhreleitung), Teploenergetika 1 (4) (1954) 40–44.
- [58] H.H. Al-Kayiem, A. Bin Ekhwan, L.N. Muhi, Augmentation of ribs turbulators height on the hydrothermal performance of double pipe heat exchanger, J. Eng. Sci. Tech. 12 (2) (2017) 548–563.